SEMARAK ILMU PUBLISHING

Journal of Advanced Research in Applied Mechanics

Journal homepage:
https://semarakilmu.com.my/journals/index.php/appl_mech/index
ISSN: 2289-7895

Design of Vibration and Turbulence Alert System for Headwater Phenomena

Muhammad Amirul Hisham Razian[1], Herdawatie Abdul Kadir[1,*], Ahmad Aiman Abd Muttalib[1], Mohd Adib Mohammad Razi[2], Babul Salam Ksm Kader Ibrahim[3]

[1] Fakulti Kejuruteraan Elektrik dan Elektronik Universiti Tun Hussein Onn Malaysia, 86400 Parit Raja, Batu Pahat, Johor, Malaysia
[2] Fakulti Kejuruteraan Awam dan Alam Bina Universiti Tun Hussein Onn Malaysia, 86400 Parit Raja, Batu Pahat, Johor, Malaysia
[3] Department of Electrical and Computer Engineering, College of Engineering and Architecture, Gulf University for Science & Technology, Masjid Al Aqsa Street, Mubarak Al-Abdullah P.O.Box 7207, Hawally, Kuwait

ARTICLE INFO

Article history:
Received 20 March 2024
Received in revised form 15 May 2024
Accepted 29 May 2024
Available online 30 June 2024

Keywords:
Headwater; ODAS; Vibration; Turbulence; IoT Monitoring; LoRa; ThingSpeak

ABSTRACT

The deteriorating state of ecosystems poses risks for nature enthusiasts in forests and rivers. The hazardous headwater phenomenon, a frequent and potentially fatal occurrence, threatens human life and the environment. Recognizing the danger is challenging, as existing technologies focus on flow pattern analysis rather than identification. To address this gap, the Headwater Phenomenon Warning and Monitoring System, an IoT and mobile application, was developed. Integrating sensors like accelerometers, vibration, and rain detection, the system enables real-time monitoring and provides early warnings. The prototype contributes to early warning, flood forecast, hydrological research, climate impact assessment, disaster management, and environmental monitoring, aiding our understanding of climate change implications. The prototype underwent multiple DOE to validate sensor and communication system integrity and stability. Turbulence and vibration graphs were successfully recorded, enhancing hazard identification and real-time monitoring capabilities.

1. Introduction

1.1 Physical Sensor Applications for Detection and Alert

The study proposes a low-cost, multi-sensor system as an alternative to image sensing systems for monitoring the hydrological state of temporary streams in mountainous headwaters. While image sensing systems have their benefits, they may not be able to provide an immediate response to warn of hazards during high rainfall or air humidity events. The multi-sensor system can gather real-time data on water level, flow velocity, temperature, and other parameters. It offers early warning for potential hazards like flash floods and aids in predicting future stream conditions.

* *Corresponding author.*
E-mail address: watie@uthm.edu.my

https://doi.org/10.37934/aram.119.1.174192

With its low cost and multiple sensing capabilities, this system could be utilized in resource-constrained areas where traditional monitoring methods are not feasible.

Additionally, the study acknowledges the PairwiseIHA by Chen *et al.,* [1], an open-source Python toolkit that enables users to obtain the Indicators of Hydrologic Alteration (IHA) from inflow and outflow time series for headwater reservoirs. The IHA measures derived from inflows and outflows provide insights into how reservoir operation impacts various aspects of hydrological conditions. However, while the PairwiseIHA offers valuable analytical statistics, it does not identify or alert users to potential dangers. Thus, the proposed low-cost, physical multi-sensor system complements the PairwiseIHA by providing a comprehensive monitoring solution for assessing the hydrological state of temporary streams in mountainous headwaters.

The proposed low-cost, multi-sensor system offers a promising solution for monitoring temporary streams in mountainous headwaters. However, there is a lack of research on its accuracy, reliability, and performance in adverse conditions. Further studies are needed to assess its effectiveness and identify any limitations, as well as to explore potential improvements for practical deployment in resource-constrained areas. This gap underscores the importance of empirical validation and refinement of the proposed system to advance hydrological monitoring in headwater regions.

1.2 Reliable Water Turbulence and Vibration Data Monitoring

A real-time monitoring system integrated with a multisensory system is proposed as an effective solution for assessing and monitoring headwater characteristics. The system aims to gather data in real-time and provide corrective procedures based on the collected information. The Blynk platform as conducted by Groot *et al.,*[2], although popular, lacks advanced analysis features, making it unsuitable for this purpose. Instead, the Thingspeak platform, known for monitoring and analysing system data, is suggested. The readings of sensor modules also can change and fluctuate for a variety of reasons, depending on the environment or the conditions of the sensor being placed or integrated. The study works of Adriman *et al.,* 2022 [3] indicate that the goal of a sub-system evaluation being implemented is to test the accuracy of every component used in the hardware, such as the sensors connected to the microcontroller. The system will be tested in a small mountainous headwater catchment during the rainy season, monitoring water vibration, turbulence, and temperature. Sensor modules are crucial for collecting accurate data but require evaluation, calibration, and protection from environmental factors to ensure reliability.

1.3 Headwater

The term "headwater phenomena" refers to the sudden and rapid increase in water volume, turbulence, and velocity that occurs in upper reaches of a river. This phenomenon plays a critical role in the formation of micro- and macro-watersheds, which are essential for maintaining downstream water quantity and quality, referred by Hayashi, 2020 [4]. Headwaters are also a significant source of multiple nutrients for downstream systems as described by Fovet *et al.,* 2020 [5].

One of few cases which cause extensive damage is the flash floods and headwater that occurred in Kedah's Yan district due to heavy rain in the upstream and highland areas covered by Bernama, 2021 [6]. The intense rainfall prevented water absorption into the ground, causing overflow as tree roots and catchment areas couldn't hold the excess water.

Headwater catchments are typically composed of various components, including the valley head or swale, depending on the surface types. The best position for placing the monitoring devices was

determined using rapidly varied flow analysis. Hydraulic analysis was conducted, and the river's behaviour at various points was studied, considering variations in water surface elevation and flow characteristics. An optimal location with more uniform flow patterns was identified, ensuring survivability of the prototype. As for water turbulence, various water flow conditions with different velocities to represent different Reynolds numbers. The sensor readings (vibration and accelerometer data) from the prototype will determine each flow condition when calibrated with Reynolds number.

1.3.1 Rapidly varied flow

The principles of rapidly varied flow may be derived by considering the water flowing in an open channel. The general Bernoulli constant for an open channel is. Consider point A in an open channel where the fluid is flowing with velocity, *V*. Let the height of the fluid above a datum line be *h*, the depth of the fluid is d, and the pressure at point A be *p*. According to Bernoulli's principle, the total head at point A is constant along a streamline. Therefore, total head at point A expressed as:

$$\mathrm{H} = z + \mathrm{h} + \mathrm{D} \tag{1}$$

$$H = z + h + \frac{p}{\rho g} + \frac{V^2}{2g} \tag{2}$$

$$H = z + D\ \frac{V^2}{2g} \tag{3}$$

where *H* is the energy of the fluid according to J. Lindell *et al.,*[7] with respect to an arbitrarily chosen datum plane, D is depth and z is the elevation head. The behaviour of Rapidly Varied Flow (RVF) is significantly influenced by the headwater. The position, size, and behaviour of hydraulic leaps and other RVF characteristics are strongly influenced by the headwater height.

1.3.2 Water turbulence

To have a better understanding of water turbulence. Reynolds number (Re) is a dimensionless parameter used in fluid dynamics to determine the type of flow regime a fluid is experiencing. It was introduced by Osborne Reynolds, a British physicist and mathematician, in the late 19th century. Reynolds number is calculated using the following formula from [8]:

$$Re = \frac{\rho V D}{\mu} \tag{4}$$

where ρ is the density of the fluid, V is the velocity of the fluid, D is the characteristic length (e.g., diameter of a pipe) and μ is the dynamic viscosity of the fluid.

The Reynolds number predicts fluid flow behaviour, distinguishing between laminar and turbulent flows. It helps optimize fluid-handling equipment design in engineering applications like pipes and pumps.

1.4 Multisensory Design Selection

The study by M. A. Kameel *et al.,* 2020 [9] introduces a physical sensor application to detect headwater. The system comprises a Raspberry Pi, a sensing layer, and on-site siren devices. The Raspberry Pi monitors water level sensor data, transmitting updates to a database via the internet. The FC-28 moisture sensor is positioned at a higher level than usual to detect water presence in that area, while the HC-SR04 ultrasonic distance sensor measures the water level.

Sensor applications play a crucial role in gathering input data, but combining certain sensors can be complex. To simplify this process, sensor modules, as demonstrated in a study by A. Afzan *et al.,*[10], can be utilized. For instance, a turbine flow meter measures fluid volume and duration, employing freely hung turbine blades that rotate as fluid passes through the device's casing. The rotational speed of the rotor is proportional to the water flow speed, which is measured using a hall effect sensor. Similarly, in a study by R. Assendelft *et al.,*[11], flow meter sensors were successfully incorporated into their design, along with other sensors like ER, temperature, and float switch sensors, providing valuable information on water flow and presence. These approaches contribute to the development of efficient system designs.

However, due to the constant movement of the apparatus holding the sensor, flow meter sensors may not be practical in open channels with strong currents and so as in Figure 1, MPU6050 accelerometer were used according to G. Hoar *et al.,*[12], by replacing the conventional flow meter sensor with an accelerometer, the vibrations caused by water turbulence can be detected and measured with greater precision. SW-420 vibration sensor which the circuit will briefly be disconnected, and the output will be low when the movement or vibration takes place as documented by seeed, 2022 [13] also was added on combining with the MPU6050 in Figure 2.

The YL-83 rainfall sensor in Figure 3 is considered a suitable option for integration as an additional sensor, as headwater conditions are often prevalent during rainy seasons. The sensor operates as a switch when a raindrop passes through the rainy board and can measure the intensity of the rain. The module consists of a separate rain board and control board for greater convenience, a power indicator LED, and a potentiometer with adjustable sensitivity as stated in the documentation of Kernbach. S *et al.,*[14].

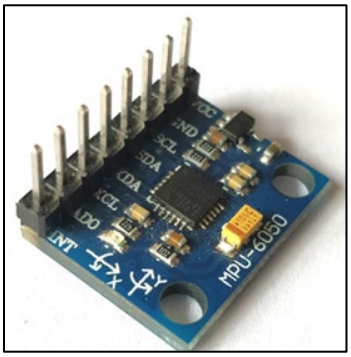

Fig. 1. MPU 6050 accelerometer sensor [12]

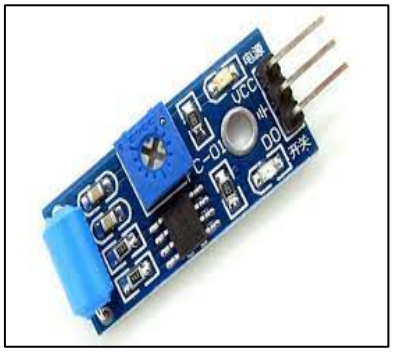

Fig. 2. SW-420 vibration sensor [13]

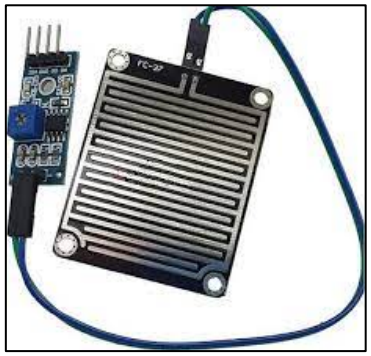

Fig. 3. YL-83 rainfall sensor [14]

1.5 Communication Protocol

The transmitter's technology must be dependable and capable of transmitting data without the use of an internet connection. This is due to the possibility that building internet connections would not be feasible where the studies were conducted. Additionally, the vast bulk of the mountainous or

hilly regions lack internet access. The device must be able to transmit and receive data without the use of the internet to solve the problem. The most suitable device is the LoRa RF module as in Figure 4.

Fig. 4. LoRa RF module

The term LoRa ("long range") refers to a specific, exclusive radio communication method. Based on chirp spread spectrum (CSS) technology, it uses spread spectrum modulation techniques referring to Semtech, 2019 [15]. Together, LoRa and LoRaWAN define a Low Power, Wide Area (LPWA) networking protocol that focuses on key Internet of Things (IoT) requirements like bi-directional communication, end-to-end security, mobility, and localization services and is designed to wirelessly connect battery-operated devices to the internet in regional, national, or global networks. As opposed to a wireless WAN, which is intended to connect people or organizations and transmit more data while consuming more power, this sort of network is low power, low bit rate, and IoT enabled. The LoRaWAN data rate per channel is between 0.3 and 50 kbit/s as per mentioned by F. Adelantado *et al.,* 2017 [16]. LoRa operates on the 2.4 GHz range worldwide and the license-free sub-gigahertz radio frequency bands EU868 (863-870/873 MHz), AU915/AS923-1 (915-928 MHz), US915 (902-928 MHz), IN865 (865-867 MHz), and AS923 (915-928 MHz) by Kjendal. D, 2021 [17].

1.6 Prototype Modelling

In this study, the system will be installed in a flowing river, which will make it difficult to develop the system's model. Consequently, it is crucial to understand the model's properties. In the modelling phase, the main concern is whether the system can be represented as a fixed prototype or a detachable prototype.

Referring to the work of Afzan. A *et al.,* 2020 [18], using an aluminum shaft, a drone will be equipped with a sonar depth sensor and a Hall Effect turbine flow meter to detect the flow velocity. The equipment is flown to the location via drone. At the time of measurement, the drone is lowered and both sensors are submerged in water. This design falls within the mobile or detachable categories. This concept is appropriate for areas that are difficult to access, congested, with insufficient room for prototype development, and occasionally have rough earth structures.

However, if the study or experiment area consists of sufficient room for prototype development, easy access and decent earth structures, the work by Assendelft. R *et al.,* 2019 [19] which the crossbar, which was hammered into the stream bank, was fastened to the angle bar, which was hammered into the streambed with its angle pointing upstream.

2. Methodology

2.1 System Design

The entire control process of the prototype was established using the Arduino IDE integrated with the ESP32. As shown in Figure 5, the system's initial step is to establish a connection between the LoRa module and the gateway. The system uses three different sensors, including a rainfall sensor (YL-83), an accelerometer (MPU-6050), and a vibration sensor (SW-420), which continuously monitor their respective parameters. Whenever the YL-83 detects heavy rainfall, the MPU-6050 detects heavy orientation, and the SW-420 detects heavy vibration, the system will evaluate if all three sensors have met the required condition. If the condition is met, the system will activate, and the LED indicator will start to blink red.

The system will then use the LoRa module to transmit data to the gateway over the LoRa network which ensures reliable and secure communication over long distances. Once the gateway receives the data, it will be displayed on an OLED screen, allowing for easy visualization of the system's status and data.

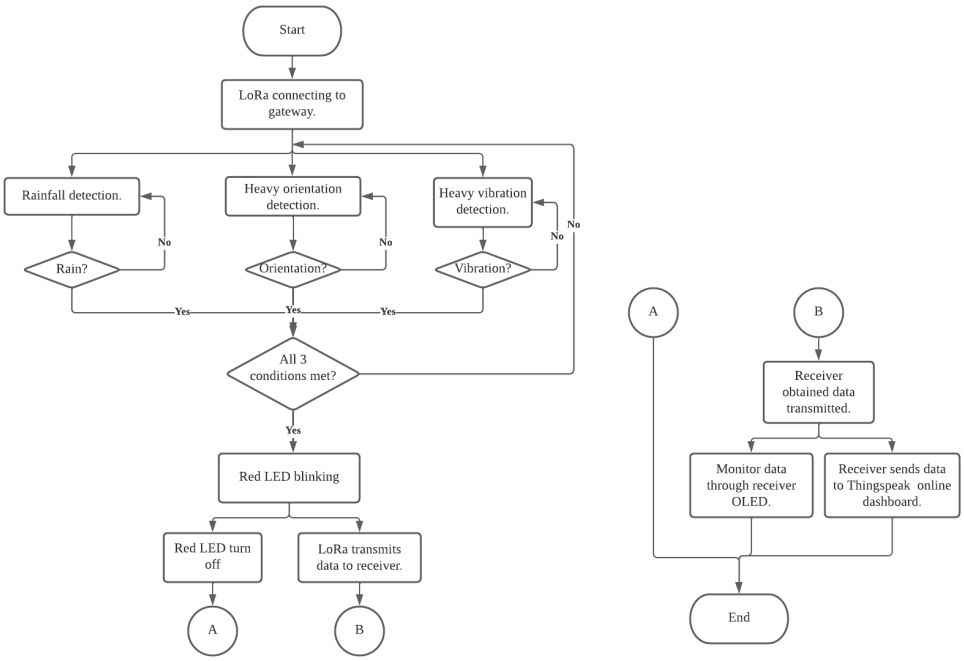

Fig. 5. Overall system process

2.2 Circuit Design

In the transmitter circuit in Figure 6, it consists of several circuit combinations which is the sensor combination and also LoRa transmitter. The data from the sensor will be processed and controlled by the ESP32 MCU. As all the conditions of the sensor are fulfilled, the alert notification will be sent and at the same time, the LoRa transmitter fetches the data to be transmitted.

However, numerous initializations must be completed before the LoRa connection can be created, including the "AT+ADDRESS" setting of the address. The ADDRESS is regarded as the transmitter's or a receiver's specific identity. The next step is "AT+BAND," which sets the wireless band's central frequency. To communicate with one another, the transmitter and receiver must be using the same frequency.

In the receiver circuit in Figure 7, the Lora receiver connected to the ESP32 to fetch sensor data from the receiver. As the Thingspeak applications do need Wi-Fi connections, this receiver unit will not be placed at the site due to limitations of internet connections. However, this receiver unit is to be placed somewhere with strong internet connections for monitoring the data. The range will not be a problem as the LoRa module can transmit data for around 10 kilometres with correct settings.

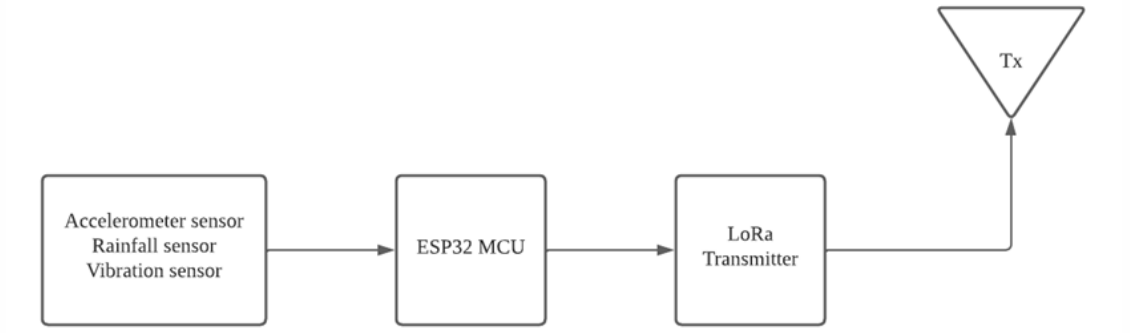

Fig. 6. Transmitter circuit block diagram

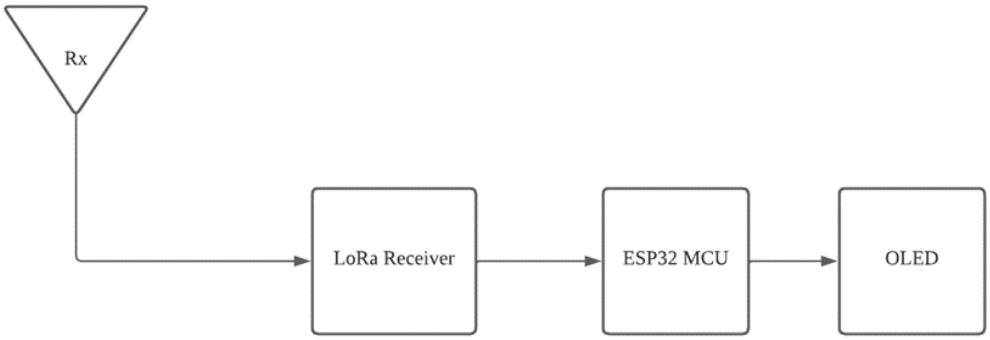

Fig. 7. Receiver circuit block diagram

Referring to Figure 8, the vibration sensor is connected to digital pins while the rain sensor and accelerometer sensor use analog pins in order to transfer data. The LoRa module TX pins are being connected to the TX pins at the ESP32 board. The LED in the circuit acts as an indicator when the headwater alert is being transmitted. Figure 10 shows the implementation in a project box, where will be rubber sealed when closed. The switch and charging port will be covered by a lid to avoid water and moisture from entering the circuit.

The construction of the receiver circuit is simple as shown in Figure 9. The circuit only consists of ESP32, OLED and only LoRa receiver. The RX connections of the LoRa module are connected to the RX pin on the ESP32 board. Figure 11 shows the implementation in a smaller project box which is powered by USB connection.

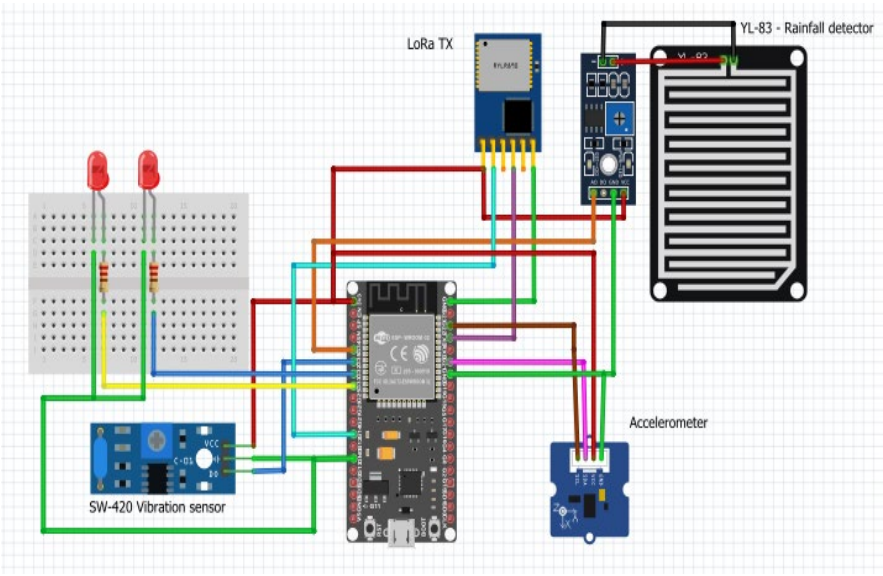

Fig. 8. Transmitter schematic diagram

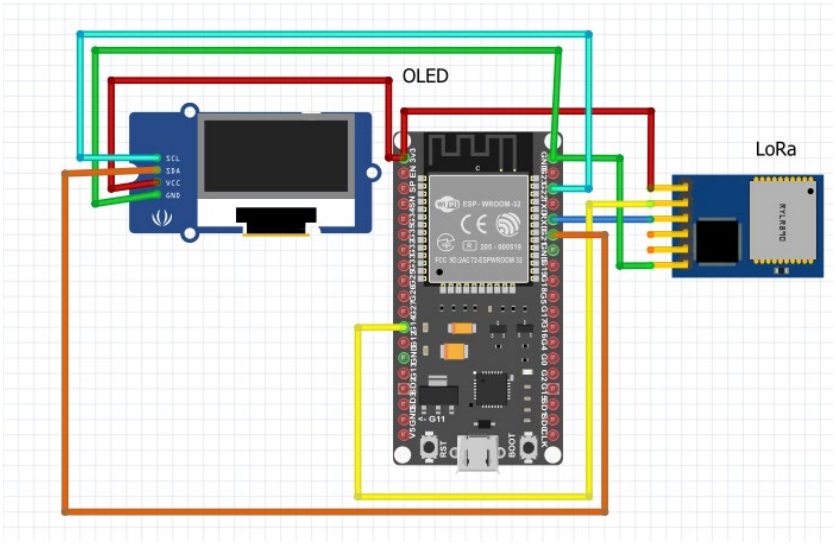

Fig. 9. Receiver schematic diagram

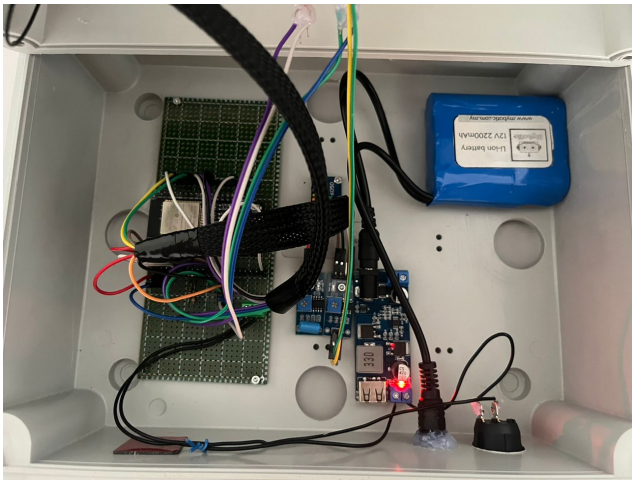

Fig. 10. Transmitter circuit

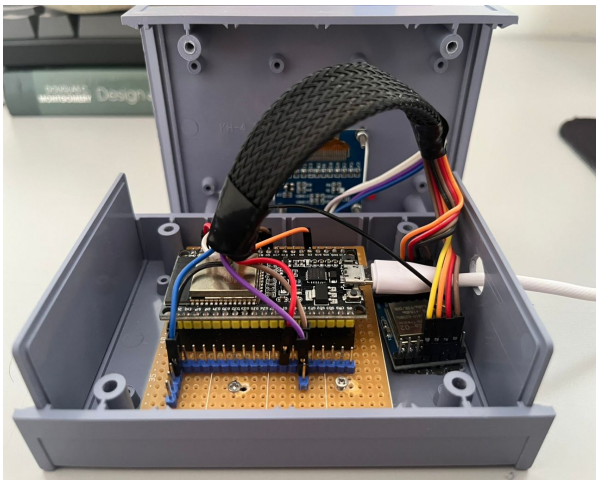

Fig. 11. Receiver circuit

2.3 Buoy Design

A buoy intended to gather information about the ocean environment is known as an ODAS buoy, which stands for Ocean Data Acquisition System buoy. In most cases, these buoys are equipped with a variety of sensors that can gauge things like water temperature, salinity, wave height, and wind speed. Numerous uses for the information gathered by ODAS buoys include monitoring marine ecosystems, oceanographic research, and weather forecasting. From Figure 12,13 and 14, a design inspired by a cylindrical ODAS buoy with a large base was created using Tinker cad.

The design features a rounded cylinder shape with a wide base to provide stability in rough waters. A housing unit is included at the top of the cylinder to accommodate sensors and other equipment, with access points for wiring and other connections. Overall, the design is practical and functional, with a focus on stability, durability, and ease of use in marine and river environments.

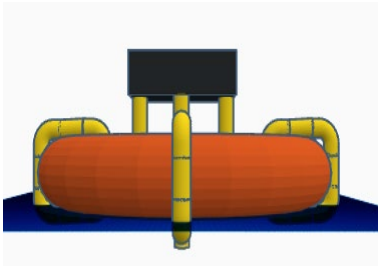

Fig. 12. Front view

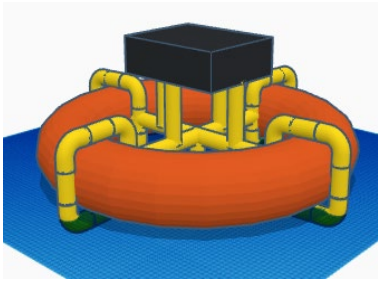

Fig. 13. Isometric view

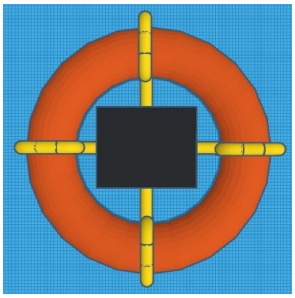

Fig. 14. Top view

PVC pipes are widely available through various hardware shops, making it a convenient and accessible material for developing buoy frames. This availability and accessibility make PVC pipes a preferred option for water safety equipment manufacturers and users alike. Additionally, the versatility of PVC pipes allows for customization and adaptation to meet specific requirements for different water safety applications.

Furthermore, the ease of assembly of PVC pipe frames, as demonstrated in the provided materials list in Table 1, enables quick and efficient production, reducing lead time for delivery and installation. In summary, the combination of PVC's desirable properties and its availability through various hardware shops make it a highly practical and popular material for developing buoy frames for water safety.

Table 1
List of materials needed to build buoy's frame

Material	Quantity
PVC Safety buoy	1 unit
PVC pipe 20mm (thick)	3m
PVC 90° 20mm elbow	16 units
PVC Tee 20mm socket	8 units
PVC 4-way connector	1 unit

Based on Figure 15, The buoy frame has a total length of 75 cm, with a frame arm length of 44 cm. The pillar to holder length is 18 cm and 13 cm, respectively. These dimensions have been chosen based on the specific requirements of the project and may vary depending on the intended use and design specifications. The size and length of the buoy frame are important considerations when designing a buoy for water monitoring applications. The frame should be large enough to support the required sensors and electronics, while also being compact enough to be easily transported and

deployed in the water. Additionally, the length of the frame arms and pillars should be carefully considered to ensure that the frame is stable and can withstand the forces of the water. The buoy frame in Figure 16 consists of a pillar at A with a length of 15 cm and a holder, B with a length of 18 cm. The height of the holder, C, is 18 cm as well.

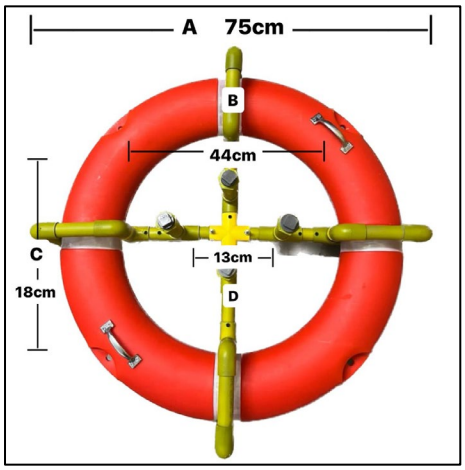

Fig. 15. Dimension of buoy frame

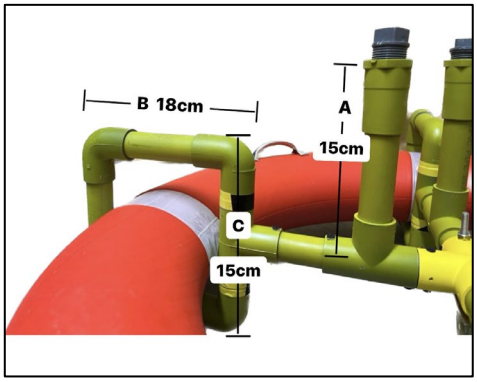

Fig. 16. Dimension of pillar and holder

Although the prototype is designed to be lightweight and durable, its lightness can pose a challenge when it comes to keeping it anchored in place. The risk of it drifting away with the water turbulence can compromise the stability and accuracy of the prototype, rendering it less effective. To address this issue, a strong anchor is required to secure the prototype in the desired location. In addition to a strong anchor, a reliable hook is also necessary to keep the prototype in place. The hook must be able to withstand the forces exerted by the water, while remaining attached to the frame. A wall hook has been selected as the appropriate solution, as it provides a sturdy and secure attachment point for the anchor. The wall hook is being connected by bolts and nuts to attach it to the centre beneath the frame as in Figure 17.

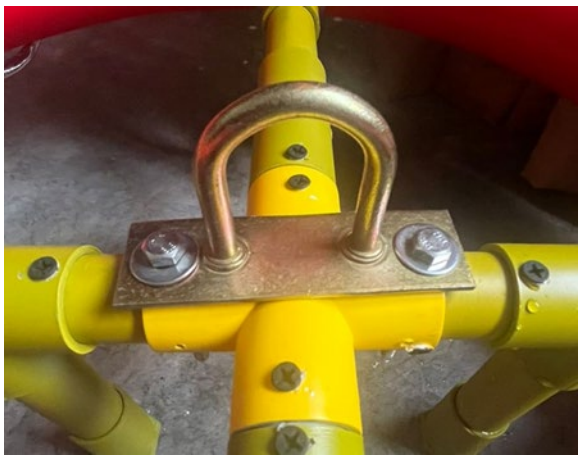

Fig. 17. Wall hook used for anchor point

The prototype design consists of a transmitter and receiver system as in Figure 18 and Figure 19 that enhances the capabilities of the ODAS buoy. On the receiving end, the prototype features a highly ranged Lora connection, enabling seamless communication with the buoy. This connection provides internet access for real-time data monitoring and storage. Additionally, an OLED display is

incorporated into the receiver, enabling the visualization of alert messages. This allows users to stay informed about critical events or changes in the monitored area.

Fig. 18. Buoy with transmitter box

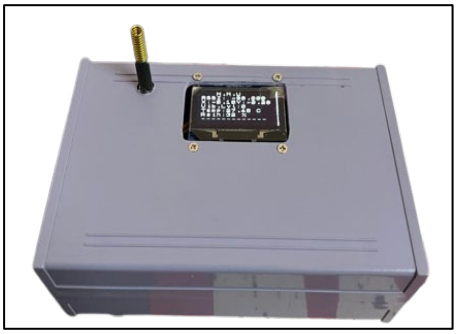

Fig. 19. Receiver and monitoring unit

3. Results

3.1 Distance impact on RSSI

When more than one input component is thought to have an impact on an output, DOE is used to enable wise decision-making, it was created to enhance the quality control process that could be utilized to research how design factors affect system status K.Vanaja *et al.,* 2007 [20].The DOE experiment was conducted at the lake in front of FKEE, where the prototype was placed to test the LoRa. The transmitter was placed at a lower altitude than the receiver due to the altitude of the lake. The initial reading of the RSSI was taken as in Figure 20, and then the distance between the transmitter and receiver were varied while moving the receiver away from the transmitter. The distance was recorded, and 20 samples were taken in a random order to reduce any bias in the experiment.

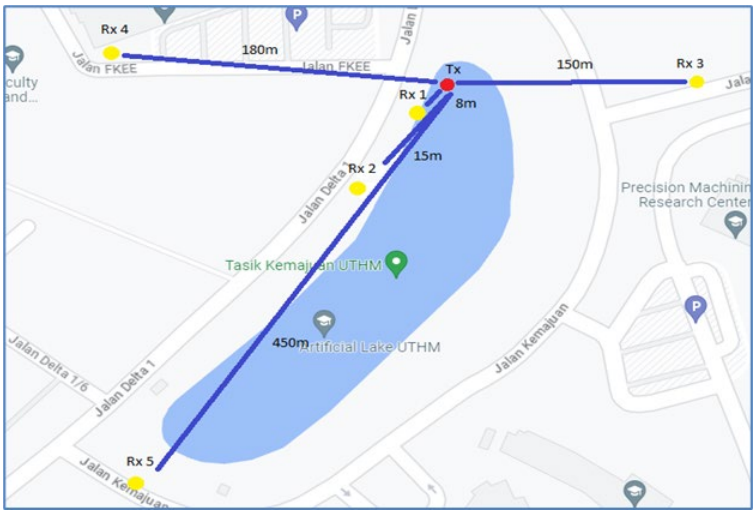

Fig. 20. Distance of five receiver samples from the transmitter

Table 2 shows the results of measuring the received signal strength indicator (RSSI) in decibel-milliwatts (dBm) for several ranges of distances between the transmitter and receiver in a LoRa system. In this experiment, the use of random data is important to ensure that the results obtained are representative of the overall population being studied. The randomization process helps to reduce bias and control the effect of extraneous variables that may influence the outcome of the

experiment. The RSSI values indicate the power level of the signal received by the receiver. Lower values indicate strong signal with higher values indicating weaker signals.

Table 2
Distance against signal strength RSSI

Distance (m)	RSSI (dBm)
8	-87
100	-122
200	-123
30	-112
150	-120
180	-121
10	-97
15	-100
35	-117
20	-94
90	-120
130	-121
5	-89
0.5	-67
135	-121
160	-120
350	-123
450	-123
50	-118

A normality test can be used to determine whether the data is normally distributed when studying the relationship between distance and RSSI in a LoRa communication system. The p-value for the results of the given normality test is reported to be less than 0.005 as in Figure 21. The null hypothesis, which states that the data exhibits a normal distribution, is strongly rejected by this p-value. This means that it may not be appropriate to use statistical techniques that assume normality, such as t-tests or ANOVA, because these techniques may produce biased or inaccurate results. Instead, a non-normal distribution of the data is more likely. The distance against RSSI test results in a statistically significant relationship between these variables when the p-value is less than 0. 005.The normality test is conducted to evaluate the distributional properties of the distance versus RSSI data. The results show that the mean value of RSSI is -110.65, with a standard deviation of 15.94 and a variance of 252.24. The skewness value of 1.45651 indicates that the data is positively skewed, while the kurtosis value of 1.42120 suggests that the data has a heavier tail than a normal distribution.

The boxplot data as in Figure 22 shows that the dataset has a median value of -119 dBm, with the first quartile (Q1) at -121 dBm and the third quartile (Q3) at -97.75 dBm. The interquartile range (IQR) is 23.25 dBm, calculated as the difference between Q3 and Q1. There are no outliers in the data, and the sample size (N) is 20.

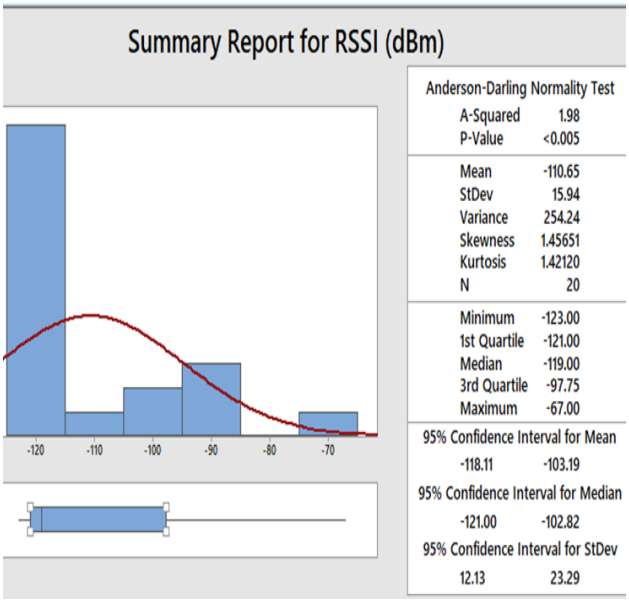

Fig. 21. Summary Report for RSSI (dBm)

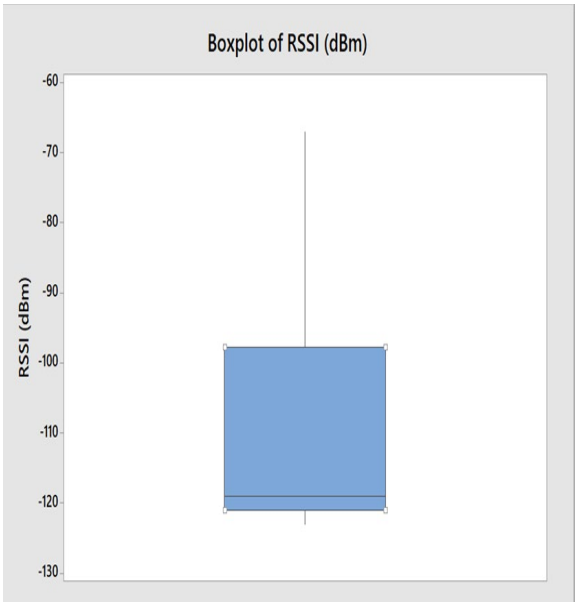

Fig. 22. Boxplot of RSSI

3.2 Object and Obstacle Impact on RSSI

In this test, the setup involved placing the transmitter at a fixed point with a radius of 10 meters. The receiver was then moved to five different object classes, including trees, glass walls, confined spaces, line of sight without any obstacles, and walls as in Figure 23. The RSSI was measured and recorded for each of the five locations. The purpose of this experiment was to observe the impact of different types of obstacles on the RSSI. The results of this experiment would help to determine the reliability and accuracy of the LoRa connectivity in real-world scenarios where different types of obstacles may exist. The received signal strength indicator (RSSI) and LoRa signal strength can be greatly influenced by the type of item and obstacle. The effect of various obstructions on the received signal strength indicator (RSSI) of a LoRa signal is discussed in Table 3. The obstacle class is shown in the first column, and the RSSI measurement for each obstacle is shown in the second column in decibels (dBm). A value of 1 indicates that the RSSI reading from the line of sight/clear was affected by the obstacle. The third column shows if the obstacle influenced the reading. In comparison to the line-of-sight condition, the results demonstrate that trees, walls, glass, and enclosed spaces all influence the RSSI reading. Among the obstacles, Trees and wall have the highest impact, with an RSSI value of -110 dBm, while Clear has the lowest RSSI value of -88 dBm.

Fig. 23. Rx blocked by different object class sample

Table 3
Obstacle impact on RSSI

Obstacle class	RSSI (dBm)	Impact (1/0)
Clear	-88	0
Tree	-110	1
Wall	-110	1
Glass	-106	1
Confined space	-106	1

As shown in Figure 24, the A-squared value in this case is 0.73 and the P-value is 0.022. The data significantly deviates from normality, as indicated by the P-value being below the standard criterion of 0.05. Furthermore, both the skewness and kurtosis values are positive, indicating that the data is positively skewed and has a distribution that is highly peaked when compared to the normal distribution. The mean and median's 95% confidence intervals are relatively large, demonstrating the significant level of uncertainty in these estimations.

The boxplot displays the distribution of a dataset with five observations based on the data in Figure 25. The bottom line indicates the first quartile (Q1) at -110 dBm, the middle line indicates the median at -106 dBm, and the top line indicates the third quartile (Q3) at -97 dBm. The box shows the middle 50% of the data. The difference between Q3 and Q1, which in this example is 13 dBm, is known as the interquartile range (IQR). The whiskers reach the lowest and highest observations that fall within 1.5 times the interquartile range of the lower and higher quartiles, respectively. In this instance, the whiskers reach -110 dBm and -88 dBm, indicating that no outliers exist outside of this range.

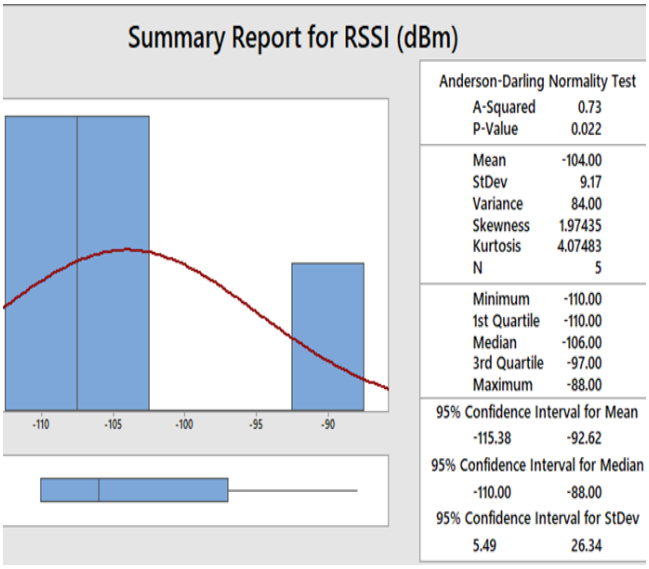

Fig. 24. Summary Report for RSSI (dBm).

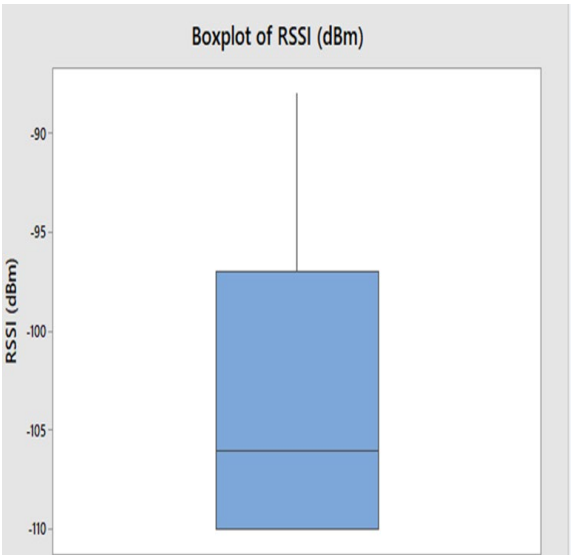

Fig. 25. Boxplot of RSSI

3.3 Temperature Effect on Accelerometer Orientation

Accelerometers are sensors that measure acceleration and are employed to ascertain an object's orientation. The temperature of the environment in which the object is located, however, may have an impact on the accuracy of the accelerometer measurements. As a result, the sensor's sensitivity is impacted, readings at various temperatures range.

In this study, the experiment setup involves placing the transmitter box at a 30° angle as in Figure 26 and was placed outside on a sunny day and initial sensor reading was taken. For the first test, the Y-axis will be at orientation while X-axis stays on its orientation plane. The second test will be otherwise. Then, the surrounding temperature will then be recorded, followed by 20 samples where the sensor from the transmitter will be recorded at different temperature readings.

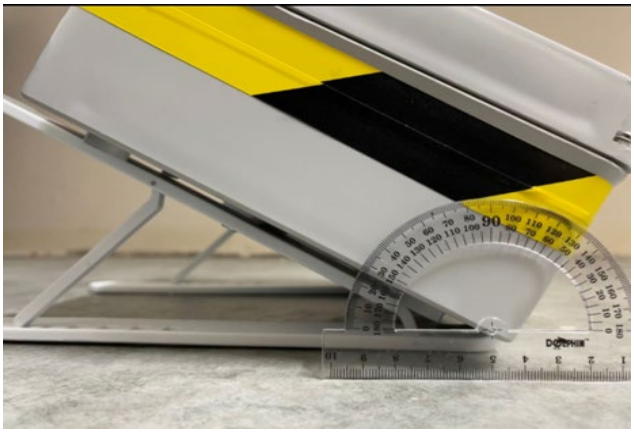

Fig. 26. Transmitter placed at 30°

The information in Table 4 illustrates how temperature affects an individual device's accelerometer's orientation. The accelerometer determines how the object is oriented in relation to the gravitational field of the Earth on its X and Y axes. The readings for both the X and Y axes were recorded, and the temperature ranged between 27.62°C and 33.19°C. The X-axis values appear to slightly change as the temperature rises, while the Y-axis values appear to slightly increase in their respective orientation. This suggests that the device's orientation, as determined by the accelerometer, is slightly affected by temperature.

Table 4
Temperature impact on accelerometer orientation

Temp (c)	X-axis	Y-axis
29.09	0.07	-4.66
29.94	0.10	-4.71
30.13	0.14	-4.73
28.94	0.07	-4.65
29.71	0.11	-4.67
28.39	0.06	-4.59
28.62	0.07	-4.68
27.62	0.01	-4.62
30.27	0.11	-4.81
30.69	0.12	-4.86
31.31	0.18	-4.84
31.87	0.08	-4.86
32.25	0.12	-4.85
33.19	0.10	-4.91
33.05	0.15	-4.87
33.00	0.11	-4.89
32.87	0.08	-4.87
28.85	0.05	-4.63
29.03	0.03	-4.67
29.05	0.07	-4.66

The data appears to not be regularly distributed, according to the results of the normality test shown in Figure 27. Since the p-value of 0.006 indicates a considerable variation from normality, further study may benefit such as non-parametric statistical tests or data transformation methods. The data are tightly grouped around the mean, as shown by the mean value of -4.7515 and the standard deviation of 0.1083 in the table above. The variance of 0.0117 indicates that the data points are not far apart. With a skewness score of -0.09141, the data is roughly symmetric, and a negative kurtosis value of -1.75125, the data is less peaked and has fewer outliers than a normal distribution.

According to Figure 28, the first quartile (Q1) for the X-axis boxplot data is 0.07, which means that 25% of the data is below 0.07. The middle value in the data set, the median, is 0.09, which is. Considering that the third quartile (Q3) is 0.1175, 75% of the data is below this value. The gap between Q3 and Q1, in this example 0.0475, is what is known as the interquartile range (IQR). The whiskers cover all observations within 1.5 times the IQR, including the lowest and highest observations. There are no outliers in the data set because the whiskers' range is between 0.01 and 0.08.

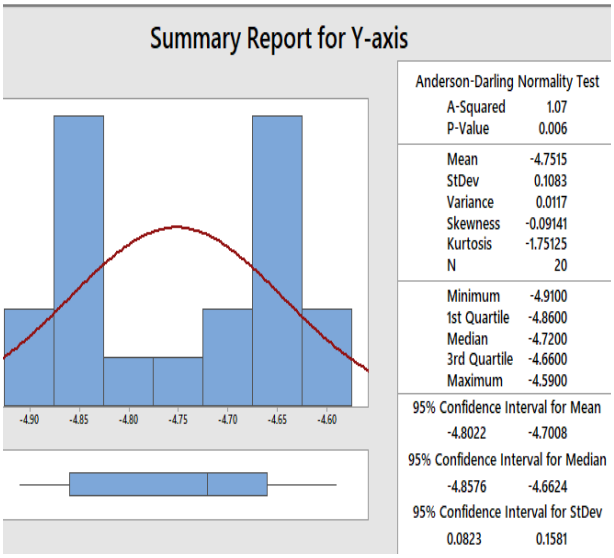

Fig. 27. Summary Report for Y-axis

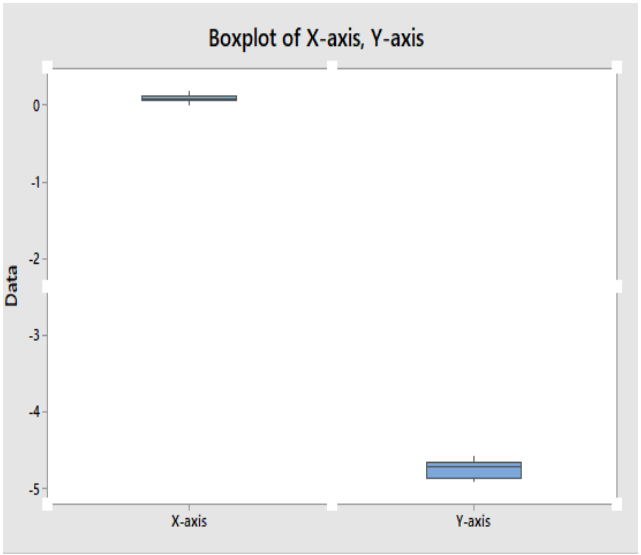

Fig. 28. Boxplot of X and Y axis

3.4 Turbulence Test

In the no turbulence test, the OLED from receiver in Figure 29 displayed consistently low values for both vibration and orientation, indicating minimal disturbance and stability in the prototype's performance, the water remains static, resulting in no movement or vibration of the buoy. The low turbulence test showed slightly higher values but remained relatively stable compared to the high turbulence test, the buoy exhibits slight movement and vibration, reflected in the data with slightly higher values. However, the overall effect remains relatively calm. In contrast, the high turbulence test displayed increased vibration and a shift in the prototype's orientation as well as displaying blinking red LED signalling the alert to the receiver. The test also exhibited a spike in the values as in Figure 30, This observation aligned with the expectation that high water turbulence would result in greater agitation and potential disruption of the prototype's stability.

Fig. 29. Low turbulence reading from receiver

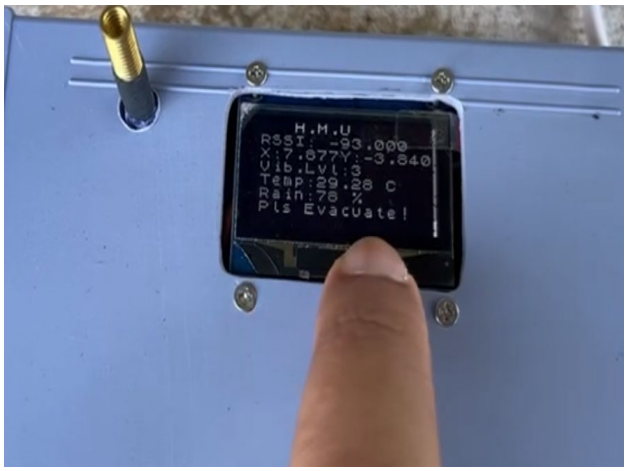

Fig. 30. High turbulence reading from receiver

The data obtained from the serial plotter in Figure 31 analysis provided valuable insights into the prototype's response to different turbulence levels. It showcased the system's ability to detect and quantify turbulence, as evidenced by the distinct variations in the plotted graph values such as in the region A is where high turbulence occurs, region B indicating there is no turbulence and only significant amount of vibration recorded by the low amplitude signal, and also region C which have low turbulence and also vibration. This data can also be viewed in Thingspeak in channel as in Figure 32 for viewing and analysing older record of the data.

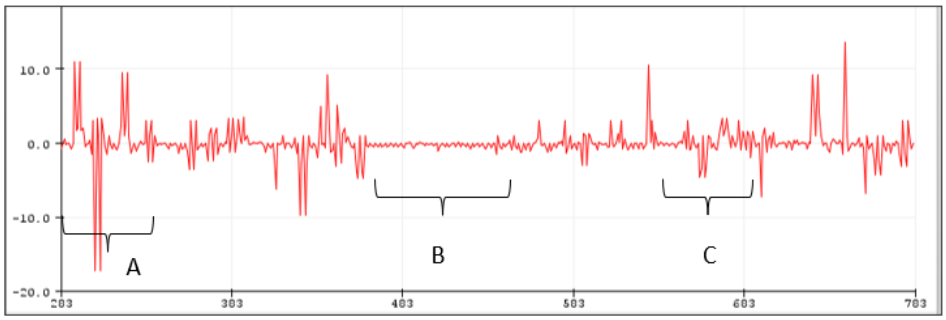

Fig. 31. Serial plotter

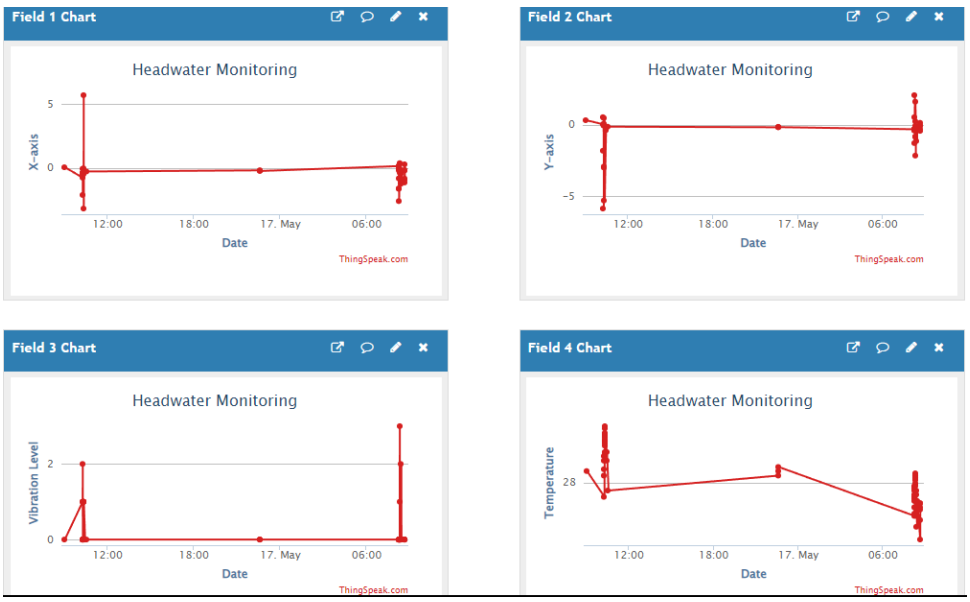

Fig. 32. Thingspeak dashboard

4. Conclusions

In conclusion, the execution of this project was straightforward, utilizing readily available materials and affordable sensors. The design of experiments (DOE) conducted in this study successfully demonstrated the influence of environmental factors on the communication protocol of LoRa and the accuracy of the sensors. The functionality test of the prototype was a resounding success, meeting all the required criteria. However, there is room for improvement in the testing venue. Moving to a real area of effect would provide more realistic velocity and water turbulence conditions, addressing the limitations imposed by the current testing facility. To mitigate these challenges, adjustments to several sensor thresholds would be necessary. By reducing these thresholds, the prototype would be better equipped to handle the environmental factors present in the testing area. Overall, this project highlights the simplicity and cost-effectiveness of the solution while acknowledging the potential for further enhancements to optimize performance in actual operating environments.

Furthermore, to enhance sustainability and address environmental concerns, integrating solar energy into the device could significantly improve its functionality and reduce its carbon footprint. Harnessing solar energy not only reduces our reliance on fossil fuels but is also beneficial for headwater projects, aiding in sustainable development while mitigating environmental degradation caused by carbon emissions as mentioned in the studies of Nabilah et al*.,* [21].

Acknowledgement

This research was supported by Universiti Tun Hussein Onn Malaysia (UTHM) through GPPS (vot Q318) and Tier 1 (vot H839).

References

[1] Chen, Zexin, Tongtiegang Zhao, Tongbi Tu, Xinjun Tu, and Xiaohong Chen. "PairwiseIHA: A python toolkit to detect flow regime alterations for headwater rivers." *Environmental Modelling & Software* 154 (2022): 105427. https://doi.org/10.1016/j.envsoft.2022.105427

[2] Groot, Tai, and Behnam Dezfouli. "Flomosys: A flood monitoring system." In *2020 IEEE Global Humanitarian Technology Conference (GHTC)*, pp. 1-8. IEEE, 2020. https://doi.org/10.1109/GHTC46280.2020.9342943

[3] Adriman, Ramzi, Maya Fitria, Afdhal Afdhal, and Alfy Yusyfa Fernanda. "An IoT-based system for water quality monitoring and notification system of aquaculture prawn pond." In *2022 IEEE International Conference on Communication, Networks and Satellite (COMNETSAT)*, pp. 356-360. IEEE, 2022. https://doi.org/10.1109/COMNETSAT56033.2022.9994388

[4] Hayashi, Masaki. "Alpine hydrogeology: The critical role of groundwater in sourcing the headwaters of the world." *Groundwater* 58, no. 4 (2020): 498-510. https://doi.org/10.1111/gwat.12965

[5] Fovet, Ophelie, David M. Cooper, Davey L. Jones, Timothy G. Jones, and Chris D. Evans. "Dynamics of dissolved organic matter in headwaters: comparison of headwater streams with contrasting DOM and nutrient composition." *Aquatic sciences* 82 (2020): 1-12. https://doi.org/10.1007/s00027-020-0704-6

[6] Bernama. (2021, August 20). Kejadian Kepala Air Disebabkan Hujan Berintensiti Tinggi. *Astro Awani*.

[7] Lindell, James E., Wade P. Moore, and Horace W. King. "Manometers." *Handbook of Hydraulics, Eighth Edition* (2018).

[8] Chanson, Hubert. *Environmental hydraulics for open channel flows*. Elsevier, 2004.

[9] Kameel, Mohamad Afiif Mohd, Ismail Fauzi Isnin, Raja Zahilah Raja Mohd Radzi, Muhammad Shafie Abd Latiff, Kamalrulnizam Abu Bakar, Hazinah Kutty Mammi, and Marina Md Arshad. "A Development of Headwater Phenomenon Warning and Monitoring System." In *2020 IEEE 5th International Symposium on Telecommunication Technologies (ISTT)*, pp. 174-179. IEEE, 2020. https://doi.org/10.1109/istt50966.2020.9279394.

[10] Afzan, A., K. V. Harikrishnan, and R. Harikrishnan. "River Mapping using Ultrasonic and Flow Meter Sensors." In *2020 Third International Conference on Smart Systems and Inventive Technology (ICSSIT)*, pp. 627-631. IEEE, 2020. https://doi.org/10.1109/icssit48917.2020.9214301.

[11] Assendelft, Rick S., and HJ Ilja van Meerveld. "A low-cost, multi-sensor system to monitor temporary stream dynamics in mountainous headwater catchments." *Sensors* 19, no. 21 (2019): 4645. https://doi.org/10.3390/s19214645.
[12] Hoar, G., D. Inglis, M. MacInnis, and S. Tobin. "An Autonomous GNSS Wave Sensor Module for Deployment on Existing Buoy Infrastructure: Comparison and Validation of Co-Located GNSS and Accelerometer Directional Wave Sensors." In *2019 IEEE/OES Twelfth Current, Waves and Turbulence Measurement (CWTM)*, pp. 1-9. IEEE, 2019. https://doi.org/10.1109/CWTM43797.2019.8955287
[13] Seeed Studio. (n.d.). *Grove - Vibration Sensor (SW-420) - Digi-Key*. Retrieved November 23, 2022
[14] Kernbach, S., Santos, S., Eisaman, E., Fonseca, J., Kamil, I., & Henrik. (n.d.). Guide for Rain Sensor FC-37 or YL-83 with Arduino. *Random Nerd Tutorials*. Retrieved December 21, 2022, from https://randomnerdtutorials.com/guide-for-rain-sensor-fc-37-or-yl-83-with-arduino/.
[15] Semtech. (2019). *LoRa Modulation Basics* . Retrieved December 20, 2022, from the Semtech website.
[16] Adelantado, Ferran, Xavier Vilajosana, Pere Tuset-Peiro, Borja Martinez, Joan Melia-Segui, and Thomas Watteyne. "Understanding the limits of LoRaWAN." *IEEE Communications magazine* 55, no. 9 (2017): 34-40. https://doi.org/10.1109/MCOM.2017.1600613
[17] Kjendal, D. (Ed.). (2021). *RP002-1.0.3 LoRaWAN® Regional Parameters*. Retrieved December 20, 2022
[18] Afzan, A., K. V. Harikrishnan, and R. Harikrishnan. "River Mapping using Ultrasonic and Flow Meter Sensors." In *2020 Third International Conference on Smart Systems and Inventive Technology (ICSSIT)*, pp. 627-631. IEEE, 2020. https://doi.org/10.1109/icssit48917.2020.9214301
[19] Assendelft, Rick S., and HJ Ilja van Meerveld. "A low-cost, multi-sensor system to monitor temporary stream dynamics in mountainous headwater catchments." *Sensors* 19, no. 21 (2019): 4645. https://doi.org/10.3390/s19214645.
[20] Vanaja, K., and R. H. Shobha Rani. "Design of experiments: concept and applications of Plackett Burman design." *Clinical research and regulatory affairs* 24, no. 1 (2007): 1-23. https://doi.org/10.1080/10601330701220520
[21] Nabilah, Nur Amira, Cheng Yee Ng, Nauman Riyaz Maldar, and Fatin Khalida Abd Khadir. "Marine hydrokinetic energy potential of Peninsular Malaysia by using hybrid site selection method." *Progress in Energy and Environment* (2023): 1-10. https://doi.org/10.37934/progee.26.1.110
[22] Ghafar, Muhammad Ariffin Abdul, and Mariyana Aida Ab Kadir. "Hospital Preparedness Towards Earthquake in Malaysia: A Quantitative Approach." *Journal of Advanced Research in Technology and Innovation Management* 1, no. 1 (2021): 23-32.